Proceedings of the Institute of Acoustics

DISTRIBUTED-MODE LOUDSPEAKER RADIATION SIMULATION

Joerg Panzer and Neil Harris, New Transducer Ltd, Huntingdon, England

INTRODUCTION

The Distributed Mode Loudspeaker is an electro-acoustic transducer based on the direct radiation of modal bending waves [1-3]. The DML mechanics are described through partial differential equations and with the help of boundary conditions for the structure and fluid. The fluid boundary is the interface between the vibrating panel surface and the pressure of the reacting medium in which the DML is embedded.

The radiation of the DML is governed by the wave-equation, which is again a partial differential equation. Acoustic boundary conditions determine the solution. The acoustic field must match the vibrating surface of the panel and other surfaces in the radiation space. In this paper we investigate the far-field radiation pattern in free space.

BENDING WAVE RADIATION

Assuming linearity, the radiating bending wave can be expressed as the superposition of plane transversal velocity waves. A single plane wave can be regarded as a sub-module in order to describe complex field patterns. Therefore let us first investigate the radiation of these sub-modules. In one dimension and normal to the panel surface a single plane bending wave may have the form (time factor $\exp(j\omega t)$ suppressed) [2]:

$$v(x) = A \cdot e^{-j \cdot k_b \cdot x} \qquad (1)$$

with

$k_b = \sqrt[4]{\omega^2 \cdot \mu / B}$	Bending wave number [m^{-1}]
B	Bending rigidity [Nm]
μ	Mass surface density [kg/m^2]
A	Arbitrarily constant

The generated sound pressure satisfies the wave equation and the boundary conditions of continuity at the air-panel interface. A plane transversal surface wave can only radiate if it matches to the trace of a longitudinal acoustic wave. The trace of the acoustical wave is the projection onto the panel surface.

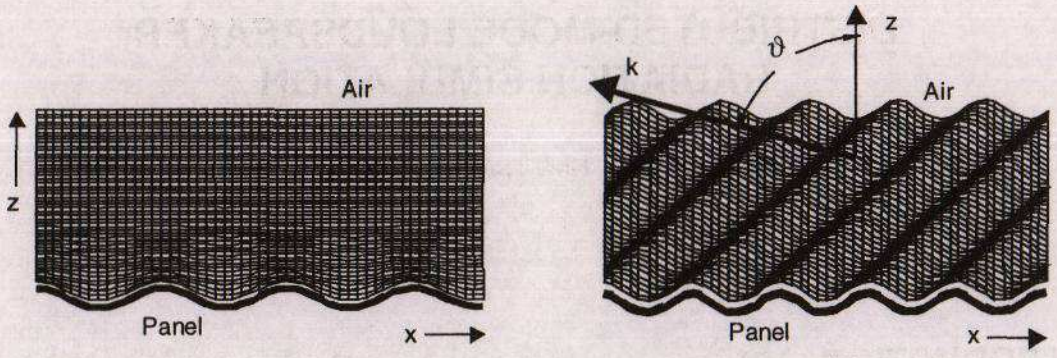

Figure 1 Plane transversal velocity wave in x direction.
Left: No radiation: $\lambda_b < \lambda_o$, Right: Radiation: $\lambda_b > \lambda_o$

Figure 1 displays a section through the panel where a bending wave travels in the x direction. Above, the grid displays the sound pressure variation. The left picture of figure 1 demonstrates the situation when the transversal bending wavelength is smaller than the wavelength in air. The air-wave cannot project a trace on the bending wave. There is only a fluctuation very near to the surface, which amplitude exponentionally decays in z-direction. Hence no real sound power is radiated.

The right picture displays the sound field above coincidence, where the bending wavelength is longer than the wavelength in air. The direction of radiation is called coincidence angle ϑ_c and is related to the speed of sound in air, c_o:

$$\sin(\vartheta_c) = \frac{\lambda_o}{\lambda_b} = \frac{c_o}{\sqrt{\omega}} \cdot \sqrt[4]{\frac{\mu}{B}} \qquad (2)$$

The frequency where the wavelength is the same for the bending wave and for the sound wave in air is called coincidence frequency, f_c:

$$f_c = \frac{c_o^2}{2 \cdot \pi} \cdot \sqrt{\frac{\mu}{B}} \qquad (3)$$

FAR-FIELD RESPONSE

The far-field response of any vibrating area in an infinite baffle is proportional to the velocity wavenumber spectrum [3].

$$p_{(R,k_o,\vartheta,\varphi)} = j \cdot k_o \cdot Z_o \cdot \frac{e^{-j \cdot k_o \cdot R}}{2 \cdot \pi \cdot R} \cdot \tilde{v}_{(k_o,\vartheta,\varphi)} \Big|_{R \to \infty} \qquad (4)$$

with

$p_{(R,ko,\vartheta,\varphi)}$	Sound pressure at frequency $f = k_o \cdot c_o / 2\pi$, listening angle ϑ, φ and distance R.
Z_o	Specific plane wave impedance $Z_o = \rho_o c_o$
ρ_o, c_o	Density and sound velocity of air
$\tilde{v}_{(k_o,\vartheta,\varphi)}$	Spatial Fourier-transform of panel velocity. Arguments mapped to listening angles ϑ and φ.

The velocity wavenumber spectrum, $\tilde{v}_{(k_x,k_y)}$, is the two dimensional Fourier transform of the radiating velocity field due to a bending wave in the x-y-plane: $\tilde{v}_{(k_x,k_y)} = \int v_{(x,y)} \cdot e^{j\cdot(k_x\cdot x + k_y\cdot y)}\, dx\, dy$. Thus the radiating velocity profile of the plate is described with the help of plane waves.

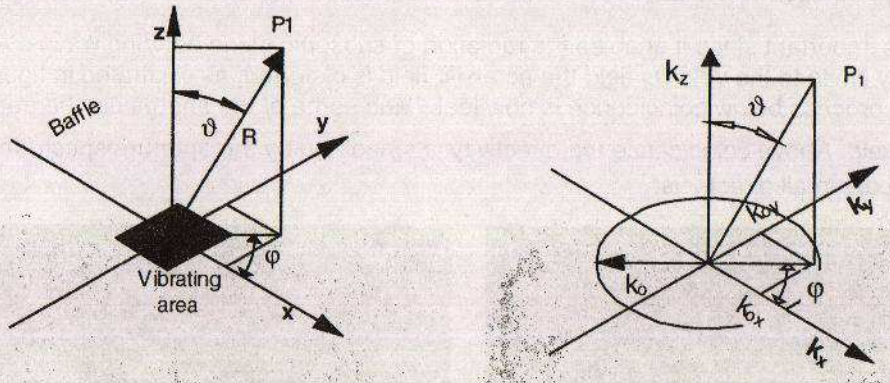

Figure 2 Left: Listening angles in space. P1: receiving point
Right: Mapping of listening angles onto k-plane

From this spatial spectrum only those wavenumber components radiate into the far-field whose k-factor is smaller than the wavenumber, k_o, as explained above. The wavenumbers are related to the listening angles ϑ and φ by (figure 2):

$$k_{ox} = k_o \cdot \sin\vartheta \cdot \cos\varphi \quad \text{and} \quad k_{oy} = k_o \cdot \sin\vartheta \cdot \sin\varphi \qquad (5)$$

On axis response gives $k_{ox} = 0$ and $k_{oy} = 0$. The maximum range which can be covered is given by the radius k_o, as illustrated in the right diagram of figure 2.

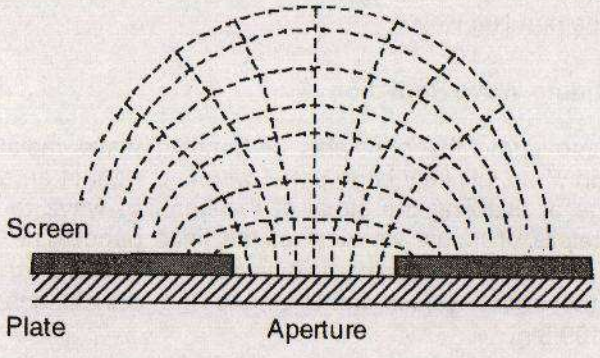

Figure 3 Aperture function $A_{(x,y)}$ on top of panel velocity function $v_{o(x,y)}$

APERTURE FUNCTION

Let us call any formulation for the mechanical velocity profile normal to the panel, $v_{o(x,y)}$. On the baffle, outside the vibrating plate, the normal component of velocity is zero, since we assume a reflecting, rigid and infinitely large baffle. Thus any formulation of the acoustic velocity profile is strictly limited to the vibrating surface. The acoustically active velocity function is therefore: $v_{(x,y)} = v_{o(x,y)} \cdot A_{(x,y)}$. We call $A_{(x,y)}$ the aperture function. $A_{(x,y)} = 1$ for x,y inside the radiating area and zero

elsewhere as illustrated in figure 3. The spatial Fourier transform of $v_{(x,y)} = v_{o(x,y)} \cdot A_{(x,y)}$ is therefore the convolution of $\tilde{v}_{o(k_x,k_y)}$ with $\tilde{A}_{(k_x,k_y)}$:

$$\tilde{v}_{(k_x,k_y)} = \tilde{v}_{o(k_x,k_y)} * \tilde{A}_{(k_x,k_y)} \qquad (6)$$

This result is important since it enables the radiation of subsonic plane bending waves. As soon as we apply any limits to the velocity field the acoustic field is distorted, as illustrated in figure 3. The cancellation process below coincidence is now leaky and some of the energy can be transduced into the far-field. Above coincidence the directivity is smoothed by the aperture spectrum $\tilde{A}_{(k_x,k_y)}$ and radiation occurs in all directions.

Figure 4 Magnitude of near-field sound pressure in front of an aperture placed over a plane bending wave (2D). Left: below coincidence. Right: above coincidence.

Figure 4 displays the near field of the sound pressure, which is created by a single plane bending wave according to equation (1) but now limited to the size of a panel. The plots display the linearly scaled sound pressure contours. The distortion of the sound field contours is clearly visible. At the bottom of the diagrams the finite vibrating panel area is symbolised with the help of an aperture covering an infinite plane bending wave.

Demonstration of Bending Wave Radiation

In order to further demonstrate the principles of bending wave radiation let us investigate an example of the radiation of an infinitely large panel with and without an aperture. This intermediate step has the advantage of enabling the study of the bending wave radiation of a finite aperture without the involved details of modal vibration of the finite panel. The material properties of the sample panel shall be such that the bending rigidity is B = 10 Nm and the mass surface density is μ = 1.015 kg/m^3. With the above values for B and μ the coincidence frequency is f_c = 6 kHz corresponding to k_c = 109.6 m^{-1}.

On the left hand side of the following series of diagrams the wavenumber spectrum is displayed. For the sake of clarity we display the properties for one dimension only. The abscissa is therefore the wavenumber k_x in the x-direction. The ordinate is the sound pressure arbitrarily scaled since the actual level is not of interest here. On the right hand side the associated polar plot according to equation (5) is displayed. The ordinate of the polar plot is arbitrarily log scaled.

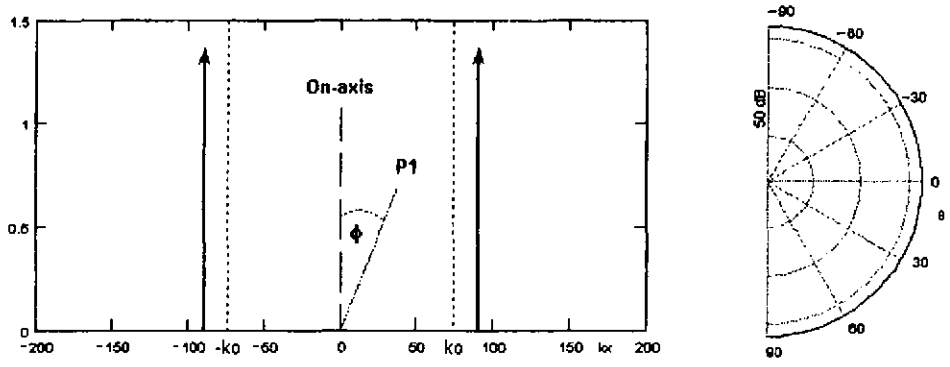

Figure 5 No aperture - below coincidence, f = 4 kHz

1. No aperture - below coincidence

In this first example let us assume a free bending wave $\cos(k_b \cdot x)$ of f = 4 kHz, which is below coincidence. k_b is marked in figure 5 with the help of two arrows, because the Fourier transform of a single plane wave is a Dirac function. No radiation can occur, which an empty directivity plot on the right hand side symbolises (see also figure 1, left diagram). According to the mapping of (5) the listening angle covers the range of k_x = -73 m^{-1} ... +73 m^{-1} while the angle ϑ runs from -90° ... +90°. The range is marked with the help of dotted lines. The given frequency, f = 4 kHz, of our free bending wave corresponds to a wave number of k_b = 89.5 m^{-1}, which is outside of the listening angle range.

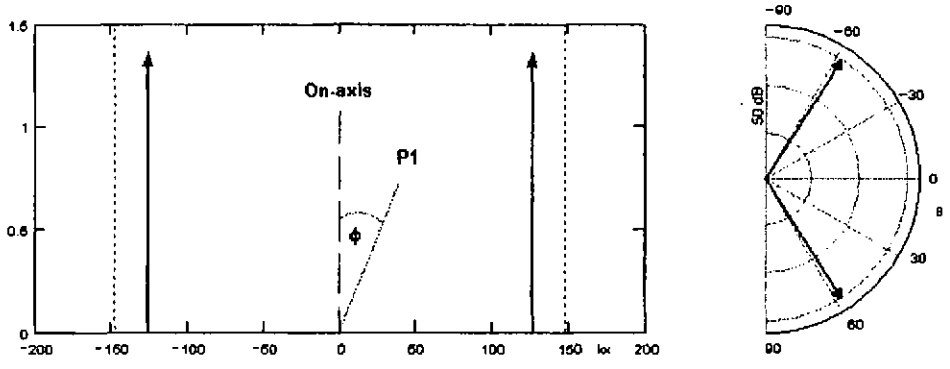

Figure 6 No aperture - above coincidence, f = 8 kHz

2. No aperture - above coincidence

In this example the free bending wave $\cos(k_b \cdot x)$ is above coincidence, at f = 8 kHz. The listening angle range now includes the two Dirac functions (figure 6). Hence a strong radiation occurs in a direction where the trace of the acoustic wave matches the bending wave of the panel (see also right diagram of figure 1).

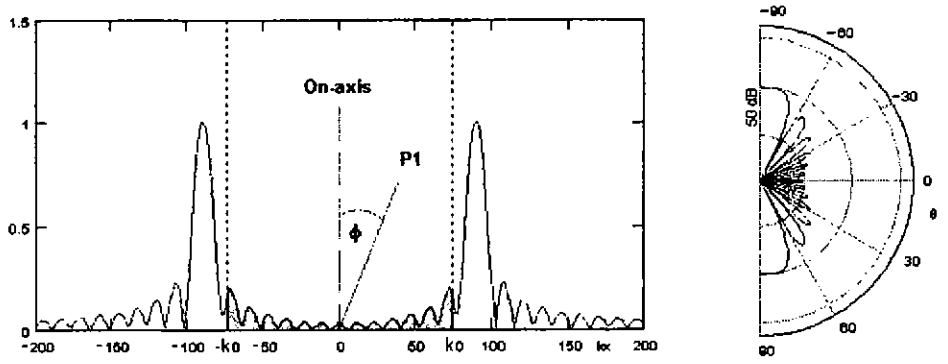

Figure 7 Large aperture - below coincidence, f = 4 kHz

3. Large aperture - below coincidence

As illustrated in figure 3 the infinite panel is now covered by an opaque screen containing a slit of width A_x = 0.5 m. We assume a plane bending wave $\cos(k_b \cdot x)$ travelling in the x-direction. The origin is placed in the centre of the aperture. In spite of driving below coincidence a far-field radiation is possible. The reason is the distorted acoustic field as sketched in figure 3. At some point, generated sound pressure can not be totally cancelled by an inverted pressure at some other point. The residual forms the radiated sound power. The power is related to the greyed zone under the curve in figure 7, i.e. exactly the range, which can be covered by the listening angle. On the right hand side of figure 7 this range is plotted again in form of the directivity plot.

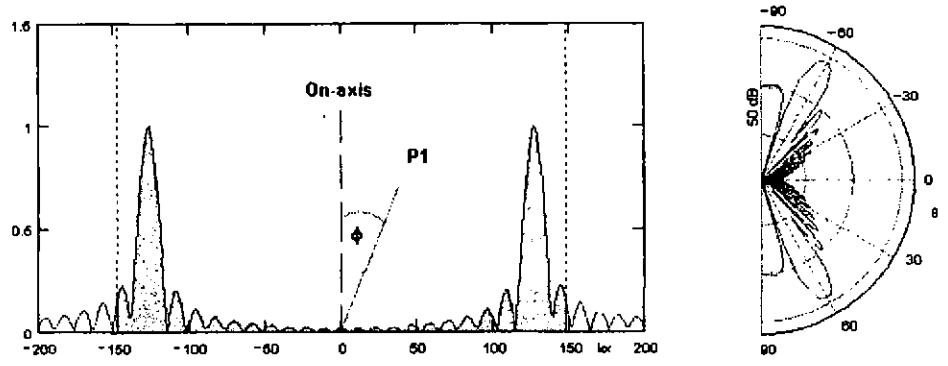

Figure 8 Large aperture - above coincidence; A_x = 0.5 m, f = 8 kHz

4. Large aperture - above coincidence

We have the same situation as in the previous example but our bending wave corresponds now to a frequency of f = 8 kHz, i.e. well above coincidence of f_c = 6 kHz. The 'coincidence beams' are within the range, which the listening angle is able to cover (greyed zone in figure 8). The Dirac functions of example 2 are now convolved with the aperture spectrum. The polar plot displays the strongly emphasised radiation at the coincidence angle ϑ_c.

Exactly at coincidence (f = f_c = 6 kHz) the range of the listening angle would end at the peaks of figure 8, i.e. the coincidence angle is in this particular case $\vartheta_c = \pm 90°$.

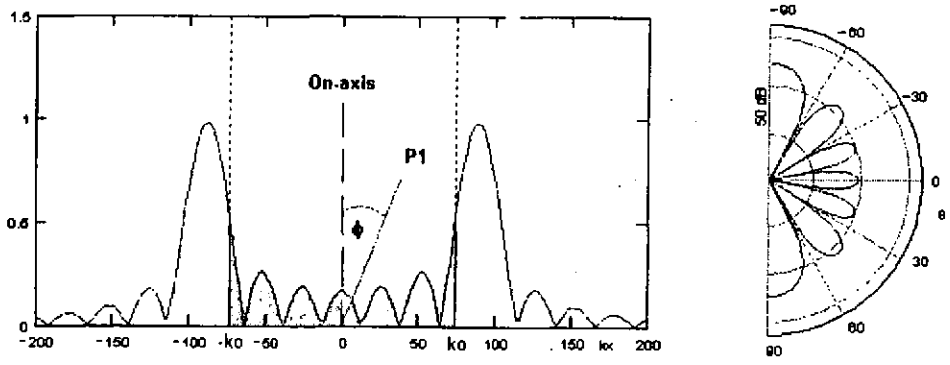

Figure 9 Small aperture - below coincidence; A_x = 0.25 m, f = 3 kHz

5. Small aperture - below coincidence

This example demonstrates the effect of the aperture-size below coincidence. The situation is the same as in example 3 but the width of the slit is halved (A_x = 0.25 m). The smaller aperture causes a stronger distortion of the acoustic field. Hence a stronger radiation can be observed as demonstrated in figure 9.

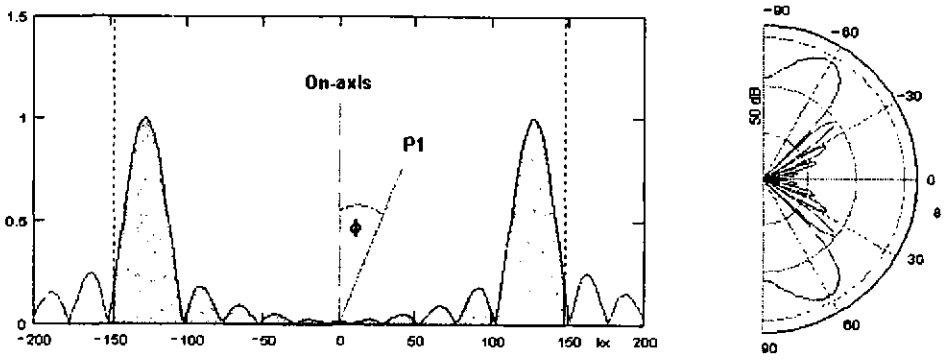

Figure 10 Small aperture - above coincidence; A_x = 0.25 m, f = 8 kHz

6. Small aperture - above coincidence

Above coincidence the effect of halving the slit width of the aperture (A_x = 0.25 m) increases the width of the coincidence beams as shown in figure 10.

By comparing the results of the examples 1 to 6 it is obvious that the aperture size controls the directivity. Below coincidence a large aperture (in comparison to the wavelength) diminishes the acoustic coupling. Above coincidence the radiated energy is focused into a certain direction called coincidence angle. Below coincidence a small aperture increases the radiation. Above coincidence the radiation in the neighbourhood of the coincidence angle is broadened.

In two dimensions the approach is similar because a plane wave travelling in any direction can always be separated into the components relating to the x and y directions. But in this case the interaction causes a smoothing of the radiation pattern.

THE FINITE PANEL

So far we have investigated the interaction of a single plane bending wave radiating through an aperture. Hence there are no reflecting bending waves and no boundary conditions to be matched. In a finite plate on the other hand, the bending wave field has to satisfy boundary conditions. For example for a finite free vibrating panel, there are no external forces and moments applied at its edges. Of course, any panel of finite size comes automatically with an 'in-built' aperture function $A_{(x,y)}$, the size of which is usually the same as that of the vibrating area of the panel. The velocity profile of a finite panel can be described with the help of a series expansion in a linear independent function system. Well-known examples are the Fourier or Hankel series where the function system consists of sin-functions or Bessel-functions, respectively. For rectangular panels an approach, which uses so-called beam-functions, has certain advantages. The beam-functions are themselves a series of sin-functions and those properties are closely related to plate mechanics. Without going into details here, we can thus always write our panel velocity profile in the form

$$v_{o(x,y)} = \sum_i \alpha_i \cdot \phi_{pi(x,y)} \tag{7}$$

with

$v_{o(x,y)}$	Bending wave velocity at point x, y
i	Mode number
α_i	i^{th} mode coefficient
$\phi_{pi(x,y)}$	i^{th} plate eigen function

The velocity profile $v_{o(x,y)}$ has to be a solution of the governing plate differential equation and has to match the boundary conditions at the edge of the panel. Both criteria determine the choice of eigen-functions $\phi_{pi(x,y)}$ and their corresponding eigen-values for each mode, i. The mode coefficients α_i are formed through the location of driving points and the coupling to mechanical and the acoustical environment. For the purpose of this paper the involved details of α_i and $\phi_{pi(x,y)}$ are not necessary (see references [5] and [6]).

As mentioned above the acoustical active velocity is $v_{(x,y)} = v_{o(x,y)} \cdot A_{(x,y)}$. Since the mode coefficients α_i are independent of x and y the only step we have to do is to apply the spatial Fourier transformation to the mode shape functions $\phi_{pi(x,y)}$, i.e.:

$$\tilde{v}_{(k_x,k_y)} = \sum_i \alpha_i \cdot \tilde{\phi}_{pi(k_x,k_y)} * \tilde{A}_{(k_x,k_y)} \tag{8}$$

Thus inserting (8) into the far-field Rayleigh formula (4), the far-field response of the finite panel in a baffle is the convolution of the Fourier spectrum of eigen-functions with the spectrum of the aperture.

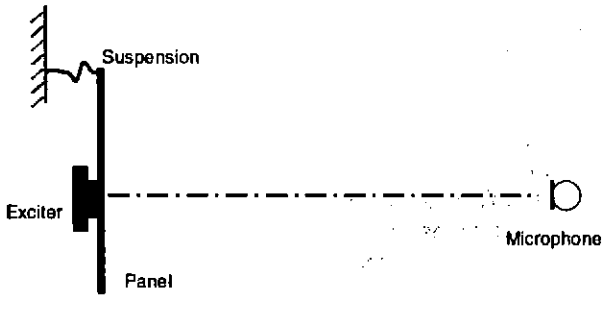

Figure 11 Setup DML simulation and measurement

Examples

A fully coupled simulation model including diffraction and interference effects, which uses the above outlined approach, has been implemented in a software tool for the design of DM loudspeaker [6].

In the following diagrams simulated sound pressure response curves are compared with experimental data. The panel used is made out of a foam sandwich structure and the dimensions are equal to A5 paper size. The coincidence frequency is approximately at f_c = 4.7 kHz. The first bending mode is around 200 Hz. The orientation is landscape. The DML is driven by a single exciter with 2 cm diameter voice coil. At the top edge the panel is suspended with two strings, otherwise the edges are free. These suspensions are modelled as two springs connecting the panel to a reference frame, as displayed in figure 11. The DML radiates from both sides. There is no baffle.

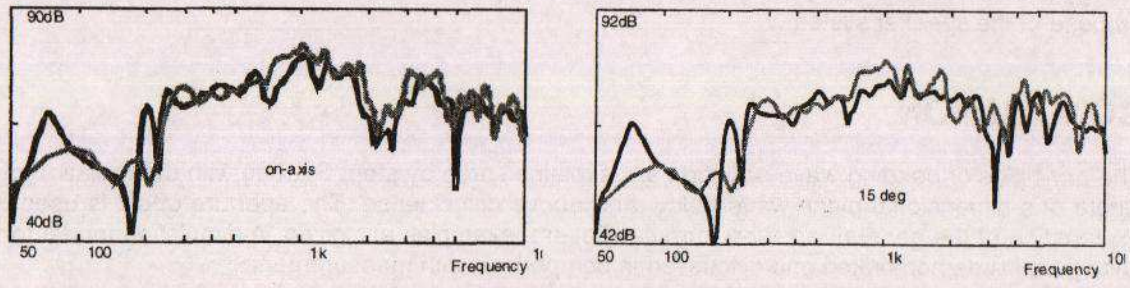

Figure 12 Sound pressure far-field response:
Left: On-axis, right: 15° horizontal;
black: simulation; grey: experimental

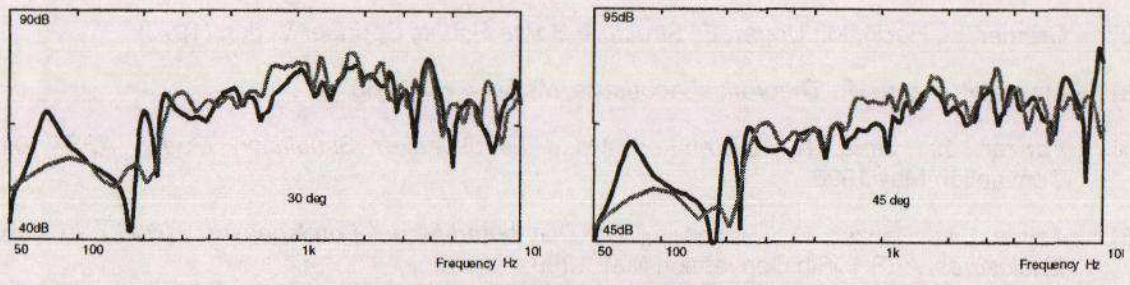

Figure 13 Sound pressure far-field response:
Left: 30°, right: 45° horizontal;
black: simulation; grey: experimental

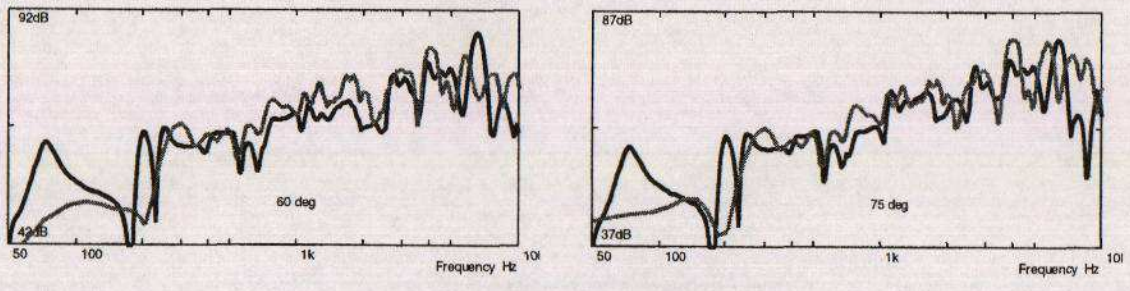

Figure 14 Sound pressure far-field response:
Left: 60°, right: 75° horizontal;
black: simulation; grey: experimental

Figures 12 to 14 display the simulated vs. measured frequency response of the sound pressure in the far-field, free from any reflections. The level range for all diagrams is 50 dB. With each diagram the microphon is rotated by 15° horizontally.

The first diagram (figure 12 left) displays the on-axis response (0°). The response starts with the first bending mode around 200 Hz and displays the typical interference pattern of a dipole type radiation at the on-axis point. At approx. 1 kHz constructive interference between the front and rear side yields an amplification. Then, around 2.5 kHz destructuive interference lowers the pressure on-axis. Above 3.5 kHz another constructive interference pattern is clearly visible.

With rotating the microphone (figures 12 right to 14 right) the interference pattern loses its contrast. Very interesting is the increase of sound pressure off-axis above 4.7 kHz which is the coincidence frequency. The used laboratory DML is designed to display this effect. However, in practice this energy is controlled by design means and modelled in such a way that the radiation pattern fits the purpose of the speaker system.

CONCLUSION

The principles of bending wave radiation are explained step by step. Starting with the radiation of a single one-dimensional plane-wave below and above coincidence. The aperture effect is used for explanation of the general radiation formula. Several examples are given. A simulation model for a finite panel is demonstrated and discussed in comparison with measurements.

REFERENCES

[1] Azima, H., *'NXT White Paper'*, New Transducer Ltd. Huntingdon PE18 6ED

[2] Cremer, L.; Heckl, M.; Ungar, E: *Structure-Borne Sound*, Springer Verlag (1973)

[3] Morse, P; Ingard U.: *Theoretical Acoustics*, McGraw Hill 1968

[4] Panzer, J.; Harris, N.: *Distributed Mode Loudspeaker Simulation Model*, AES 104th Convention May 1998

[5] Azima, H.; Panzer, J.; Reynaga, D: *Distributed-Mode Loudspeakers (DML) in Small Enclosures*, AES 106th Convention May 1999

[6] Panzer, J.; Kavanagh, S.; *Modal Network Solver for the Simulation of Complex Mechanoacoustical Systems*, AES 107th Convention September 1999